J Biomol NMR (2009) 44:157–166
DOI 10.1007/s10858-009-9325-z

ARTICLE

Two-point anchoring of a lanthanide-binding peptide to a target protein enhances the paramagnetic anisotropic effect

Tomohide Saio · Kenji Ogura · Masashi Yokochi · Yoshihiro Kobashigawa · Fuyuhiko Inagaki

Received: 6 April 2009 / Accepted: 1 May 2009 / Published online: 26 May 2009

Abstract Paramagnetic lanthanide ions fixed in a protein frame induce several paramagnetic effects such as pseudo-contact shifts and residual dipolar couplings. These effects provide long-range distance and angular information for proteins and, therefore, are valuable in protein structural analysis. However, until recently this approach had been restricted to metal-binding proteins, but now it has become applicable to non-metalloproteins through the use of a lanthanide-binding tag. Here we report a lanthanide-binding peptide tag anchored via two points to the target proteins. Compared to conventional single-point attached tags, the two-point linked tag provides two to threefold stronger anisotropic effects. Though there is slight residual mobility of the lanthanide-binding tag, the present tag provides a higher anisotropic paramagnetic effect.

Keywords Lanthanide binding peptide tag · Two-point anchoring · Paramagnetic NMR · Pseudo-contact shift · Residual dipolar coupling

Electronic supplementary material The online version of this article (doi:10.1007/s10858-009-9325-z) contains supplementary material, which is available to authorized users.

T. Saio
Graduate School of Life Science, Hokkaido University, Sapporo 001-0021, Japan

T. Saio · K. Ogura · M. Yokochi · Y. Kobashigawa · F. Inagaki (✉)
Laboratory of Structural Biology, Graduate School of Pharmaceutical Sciences, Hokkaido University, Sapporo 001-0021, Japan
e-mail: finagaki@pharm.hokudai.ac.jp

Introduction

Long-range distance and angular information is useful for the structural analysis of large proteins, multidomain proteins and protein complexes (Gaponenko et al. 2002, 2004; Battiste and Wagner 2000; Vlasie et al. 2008; Tang et al. 2006; Rumpel et al. 2007). Paramagnetic lanthanide ions induce several NMR effects on observed nuclei, including a pseudo-contact shift (PCS) and a residual dipolar coupling (RDC), due to anisotropy of the magnetic susceptibility tensor ($\Delta\chi$-tensor; Bertini et al. 2005, 2008; Otting 2008). The PCS provides distance and angular information between the lanthanide ion and the observed nuclei situated up to approximately 40 Å from the lanthanide ion (Allegrozzi et al. 2000), whereas the RDC provides molecular alignment information independent of distance (Bertini et al. 2001b; Barbieri et al. 2002). Therefore, the paramagnetic lanthanide ions are useful probes for solution structure determination by NMR and have been applied successfully to metalloproteins (Bertini et al. 2001b, 2004, 2007; Barbieri et al. 2002; Pintacuda et al. 2006, 2007; Allegrozzi et al. 2000). Metal ions such as Ca^{2+} and Mg^{2+} ions can be replaced by lanthanide ions as they share similar chemical properties. However, the application of the paramagnetic lanthanide ions to non-metalloproteins requires anchoring of the lanthanide ions to the target proteins. A wide variety of lanthanide ion anchoring tags have been developed, including lanthanide binding peptide tags (LBTs; Su et al. 2006, 2008a; Gaponenko et al. 2000; Wöhnert et al. 2003; Martin et al. 2007; Ma and Opella 2000; Zhuang et al. 2008) and synthetic lanthanide chelating reagents (Dvoretsky et al. 2002; Haberz et al. 2006; Pintacuda et al. 2004; Prudêncio et al. 2004; Rodriguez-Castañeda et al. 2006; Ikegami et al. 2004; Leonov et al. 2005; Gaponenko et al. 2002, 2004; Vlasie et al. 2007;

Keizers et al. 2007, 2008; Su et al. 2008b). These tags are attached to the target proteins through N- or C-terminal fusion (Gaponenko et al. 2000; Wöhnert et al. 2003; Martin et al. 2007; Ma and Opella 2000; Zhuang et al. 2008) or the formation of a disulfide bond with cysteine residues (Su et al. 2006, 2008a, 2008b; Dvoretsky et al. 2002; Haberz et al. 2006; Pintacuda et al. 2004; Prudêncio et al. 2004; Ikegami et al. 2004; Leonov et al. 2005; Gaponenko et al. 2002, 2004; Vlasie et al. 2007; Keizers et al. 2007, 2008). However, the mobility of the tag; i.e., the mobility of the lanthanide ion, reduces the anisotropic effect (Bertini et al. 2004, 2007; Su et al. 2008a). Therefore, tag rigidity is required for obtaining structural information using paramagnetic lanthanide probes.

The two-point anchoring method has the potential to reduce the mobility of the tag. The symmetrically designed synthetic chelators can be anchored to the protein via two disulfide bonds (Rodriguez-Castañeda et al. 2006; Vlasie et al. 2007; Keizers et al. 2007; Keizers et al. 2008). However, most of these synthetic tags are not commercially available and there is just one published tag that avoids peak doubling due to enantiomeric conformer of the lanthanide-substituted tag (Keizers et al. 2007, 2008). Meanwhile, lanthanide binding peptide tags (LBTs) are superior to these tags, in terms of availability, chiral purity and rigidity because of their bulkiness (Su et al. 2008a, b). Here, we report a method that utilizes a lanthanide-binding peptide tag, CYVDTNNDGAYEGDEL (LBT) (Nitz et al. 2003, 2004; Su et al. 2006, 2008a), linked to the target protein via two anchoring points, a disulfide bridge and an N-terminal fusion. This method was applied to the B1 immunoglobulin binding domain of protein G (GB1) as a model protein to evaluate the $\Delta\chi$-tensor of the paramagnetic lanthanide ions. We also prepared the GB1 linked to the LBT via a single disulfide bond and compared the rigidity of the tag anchored by two-points and a single point based on the size of both the $\Delta\chi$-tensor and alignment tensors obtained from PCS and RDC analysis. The results demonstrated the potential usefulness of the present two-point anchoring tag.

Materials and methods

Protocol for the two-point anchoring of the LBT to GB1

The lanthanide-binding peptide tag, CYVDTNNDGAYE GDEL (LBT), was linked to GB1 via a disulfide bridge and an N-terminal fusion as shown in Fig. 1. First, we designed the LBT fusion construct of the GB1 E19C mutant containing a 6xHis fusion tag and the tobacco etch virus (TEV) cleavage site. 6xHis was used for affinity purification and the TEV cleavage exposed the Cys residue at the N-terminus for use in the disulfide bridge formation. The position of the cysteine mutation in GB1 as well as the linker length were designed based on the structure of both LBT (Nitz et al. 2004) and GB1 (Gronenborn et al. 1991) according to the following considerations. In the crystal structure of the LBT, the distance between the C_α atoms of the N- and C-terminal residues is around 7 Å. We searched for a residue about 7 Å in distance from Met1 of GB1, and found Glu19. The C_α distance between Met1 and Glu19 was 6.1 Å. Thus we introduced an E19C mutation to GB1, and the LBT was fused to the N-terminus of the GB1 E19C mutant. A linker between the LBT and GB1 was introduced to avoid structural distortion and steric hindrance. We prepared three constructs containing one- (Thr), two- (Gly-Thr) and three-residue (Ser-Gly-Thr) linkers, respectively. The construct with the three-residue linker was selected by comparing the ^{1}H-^{15}N HSQC spectra of these constructs complexed with Tm^{3+}.

The construct with the three-residue linker was expressed using an *E. coli* expression system and purified by Ni-NTA affinity chromatography (QIAGEN) and gel filtration chromatography (HiLoad 26/60 Superdex 75 pg, GE Healthcare). Before the gel filtration chromatography, the cysteine residue at the N-terminus was exposed by TEV protease digestion. Finally, the construct was diluted to a concentration of 10–20 μM and incubated with 1 mM 5,5′-dithiobis(2-nitrobenzoic acid) (DTNB) for 2 h at room temperature to form an intramolecular disulfide bond. After incubation, DTNB was removed by dialysis. No

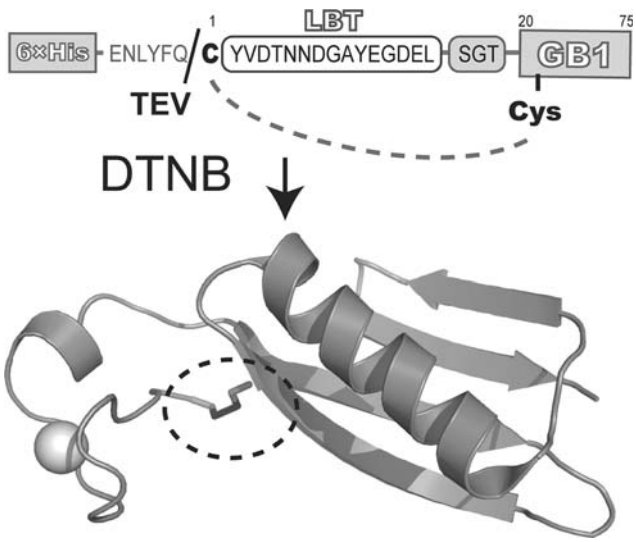

Fig. 1 Scheme of the two-point attachment of the LBT and the structure of the L2GB product determined by NMR. The L2GB contains 6xHis and the tobacco etch virus (TEV) protease cleavage site. The *sphere* in the structure represents the La^{3+} ion, and the *dashed circle* indicates disulfide bond connecting the LBT and GB1. The structure of L2GB was drawn using the program PyMOL (DeLano 2002)

intermolecular disulfide bond formation was detected by non-reducing SDS–PAGE analysis (data not shown).

Preparation of L1GB

To evaluate the mobility of the two-point anchoring tag, we also prepared L1GB, in which the LBT was attached to the GB1 E19C mutant by a single disulfide bond, based on the protocols reported by Su et al. (2006, 2008a). GB1 E19C and the LBT were prepared separately using an *E. coli* expression system. GB1 E19C was subcloned into the pET-28 vector (novagen) containing a hexahistidine-tag and a TEV cleavage site. GB1 E19C was purified by Ni-NTA affinity chromatography and gel filtration chromatography, with the removal of the hexahistidine-tag by TEV protease before the gel filtration chromatography. The LBT was subcloned into the pET-21 vector (novagen) containing a GB1 as an expression tag and a HRV3C cleavage site. A hexahistidine-tag was then fused to the C-terminus of the LBT. The LBT was purified by Ni-NTA affinity chromatography and gel filtration chromatography, and then digested by HRV3C protease. The LBT was separated from GB1 using reversed phase chromatography (RESOURCE RPC, GE Healthcare). The integrity of the LBT was checked using a MALDI-TOF mass spectrometer (Applied Biosystems). The GB1 E19C mutant and LBT were joined using DTNB as follows. First, the GB1 E19C mutant was incubated with 3 mM DTNB to form a GB1-TNB complex linked via a disulfide bond. After incubation for 2 h at room temperature, excess DTNB was removed by desalting (HiPrep 26/10 Desalting, GE Healthcare). Next, the LBT was added to GB1-TNB and incubated for 4 h at room temperature. At this step, the disulfide bond was exchanged to form GB1-LBT, henceforth referred to as L1GB. L1GB was separated from the unreacted elements using Ni-NTA affinity chromatography and gel filtration chromatography.

NMR spectroscopy and structural calculations

All NMR spectra were acquired using Varian UNITY inova spectrometers operating at 600 and 800 MHz. Both L2GB and L1GB solutions were concentrated and exchanged with NMR buffer (20 mM MES pH 6.5 50 mM NaCl). For the structure determination of L2GB in complex with La^{3+}, $^{13}C/^{15}N$-labeled L2GB with two equivalent of La^{3+} was prepared. All the NMR experiments were carried out at 295 K, as described previously (Saio et al. 2007). Data analysis was performed with the assistance of the OLIVIA program developed in our laboratory (Yokochi et al. http://fermi.pharm.hokudai.ac.jp/olivia/). The structures were calculated using the CYANA software package (Herrmann et al. 2002) based on inter-proton distance restraints from the NOESY spectra and angular restraints from the TALOS program (Cornilescu et al. 1999). In the structure calculations, La^{3+} was also introduced with eight artificial distance restraints of 2.6 Å each between the La^{3+} and the oxygen atoms of LBT; i.e., one Oε atom of Asp4, Asp6 and Asp8, two Oε atoms of Glu12, Glu15, and one main chain oxygen atom of Ala10. La^{3+} distance restraints were determined based on the crystal structure of LBT-Tb^{3+} complex (Nitz et al. 2004). One hundred structures were calculated individually using 10,000 steps of simulated annealing, and a final ensemble of 20 structures was selected based on CYANA target function values. The atomic coordinates and structural restraints for L2GB have been deposited in the Protein Data Bank, www.pdb.org (PDB code: 2rpv). Heteronuclear steady-state ^{1}H-^{15}N NOEs were obtained from a pair of NOE spectra recorded at 298 K with a 3.0 s relaxation delay, using a 600 MHz NMR spectrometer. For PCS and RDC measurement, the NMR spectra of L2GB and L1GB were acquired at 283 K in complex with the diamagnetic lanthanide ion (La^{3+}) and paramagnetic lanthanide ions (Tb^{3+}, Er^{3+} and Tm^{3+}). Aliquots of 5 mM $LnCl_3$ stock solution were added to the NMR sample. PCS values were measured as the difference in the HN chemical sifts; i.e., the chemical shifts observed in complex with paramagnetic lanthanide ions minus those observed in complex with the diamagnetic La^{3+} ion. RDC values were measured as the difference in ^{15}N-doublet splitting using the IPAP pulse sequence; i.e., the ^{15}N-doublet splitting observed in complex with the La^{3+} ion minus that observed in complex with a paramagnetic lanthanide ion.

Tensor determination from PCS and RDC

The $\Delta\chi$-tensors of L2GB and L1GB were calculated from the PCS values and the structure of L2GB and GB1 (PDB code: 1gb1; Gronenborn et al. 1991) with Eq. 1 using the Numbat program (Schmitz et al. 2008),

$$\Delta\delta^{\mathrm{PCS}} = \frac{1}{12\pi r^3}\left[\Delta\chi_{\mathrm{ax}}(3\cos^2\theta - 1) + \frac{3}{2}\Delta\chi_{\mathrm{rh}}\sin^2\theta\cos 2\phi\right], \quad (1)$$

where $\Delta\delta^{\mathrm{PCS}}$ is the pseudo contact shift, r, θ and ϕ are the polar coordinates of the nucleus with respect to the principal axis of the magnetic susceptibility tensor, and $\Delta\chi_{\mathrm{ax}}$ and $\Delta\chi_{\mathrm{rh}}$ are the axial and rhombic components of the magnetic susceptibility tensor. In the Numbat program, the metal position was refined from the La^{3+} position in the L2GB structure based on the PCS data. Conformer 1 of the family of NMR structures was used for the tensor fit.

The alignment tensors of L2GB and L1GB were evaluated from the RDC values and the structure of GB1 with Eq. 2 using the Module program (Dosset et al. 2001),

$$\Delta\nu_{\mathrm{RDC}}(Hz) = -\frac{S\mu_0\gamma_{\mathrm{N}}\gamma_{\mathrm{H}}\hbar}{8\pi^2 r_{\mathrm{NH}}^3}\left[A_{\mathrm{ax}}(3\cos^2\theta - 1) + \frac{3}{2}A_{\mathrm{rh}}\sin^2\theta\cos 2\phi\right], \quad (2)$$

where $\Delta\nu_{\mathrm{RDC}}$ is the residual dipolar coupling, S is the generalized order parameter, μ_0 is the permeability of vacuum, γ_{N} and γ_{H} are the magnetogyric ratios of ^{15}N and ^{1}H, respectively, r_{NH} is the internuclear distance between ^{15}N and ^{1}H, and θ and ϕ are the polar angles describing the orientation of the vector connecting the coupled nuclei, ^{15}N and ^{1}H. Conformer 1 of the family of NMR structures was used for the tensor fit.

Results and discussion

Optimization of the linker length in two-point anchoring

We designed the construct with two-point anchoring based on the structures of both the LBT and GB1. The linker length between the LBT and GB1 was examined from 1- to 3-residues in order to best match the distance requirements for two-point anchoring of the LBT. The ^{15}N L2GB constructs containing one- (Thr), two- (Gly-Thr) and three-residue (Ser-Gly-Thr) linkers were prepared and the ^{1}H-^{15}N HSQC spectra were acquired with 1 and 2 equivalent of La^{3+} and Tm^{3+}. As shown in Figure S1 (Supporting information), the construct with the three-residue linker showed a large PCS value with a single peak, whereas the constructs with the two-residue linker all showed double peaks. The construct with the one-residue linker also showed similar behavior (data not shown). The peak doubling in 1- or 2-residue linker might suggest that the Ln^{3+}-loaded LBT exists in two conformations or there is another weak metal binding site, due to inappropriate architecture of the tag, indicating that one- or two-residue linkers were not suitable. Thus, we concluded that the construct with the three-residue linker best matched the distance requirements and is referred to as L2GB hereafter.

The structure of L2GB

The structure of L2GB was first determined based on interproton distance restraints from the NOESY spectra and angular restraints from the TALOS program (Cornilescu et al. 1999). A total of 1488 NOE-derived distance restraints, 8 La^{3+} distance restraints and 104 dihedral restraints were used (Table 1). The overlay of 20 structures with the lowest CYANA energy and the ribbon model of the lowest energy structure are shown in Figs. 1 and 2, respectively. The structures have an average backbone

Table 1 Structural statistics for the 20 structures of L2GB

NOE distance restraints	1,488
Short range (intraresidue and sequential)	778
Medium range ($2 \leq \|i-j\| \leq 4$)	263
Long range ($\|i-j\| > 4$)	447
Dihedral angle restraints (ψ and ϕ)	104
La^{3+} distance restraints	8
Restraint violations	
Distance restraints violated by >0.3 Å	0
Torsion angle restraints violated by >3°	0
Structural coordinates rmsd (1–75)	
Backbone atoms	0.43 Å
All heavy atoms	0.73 Å
Ramachandran plot	
Most-favored regions	91.0%
Additionally allowed regions	8.5%
Generously allowed regions	0.5%
Disallowed regions	0.0%

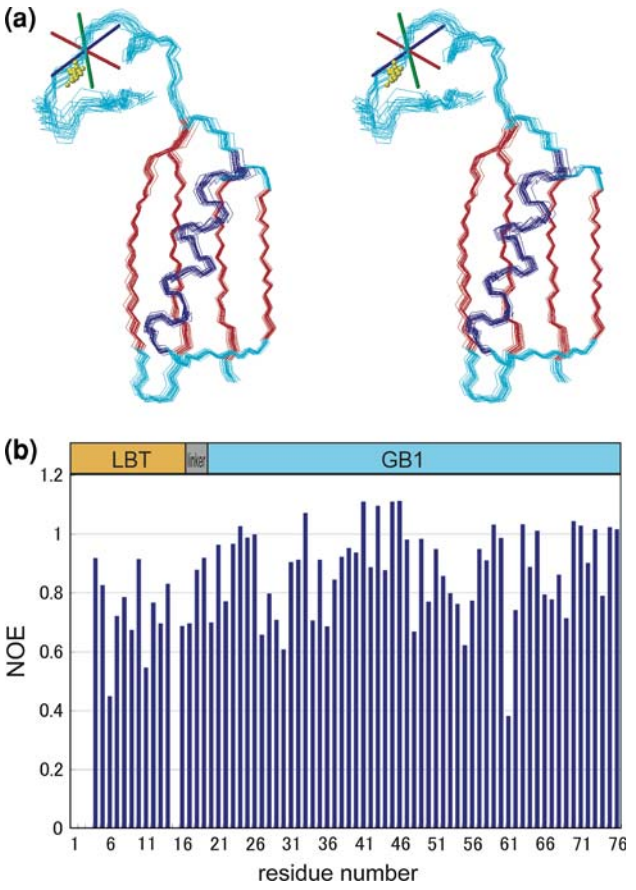

Fig. 2 Ensemble of the 20 lowest energy structures of L2GB with $\Delta\chi$-tensor axis of Tb^{3+} determined by PCS, displayed in stereo (**a**). *Yellow dots* represent the position of the Lanthanum ion. The *z*-, *y*- and *x*-axis were shown in *blue*, *green* and *red*, respectively. The structures were drawn using the program MOLMOL (Koradi et al. 1996). NOE values of L2GB in complex with La^{3+}, plotted as a function of residue number (**b**)

RMSD of 0.43 Å and they present no distance violations larger than 0.3 Å or angle violations larger than 3°. The structure of L2GB indicated that the LBT was successfully attached to GB1 via two anchoring points. In the L2GB structure, both the LBT and GB1 moieties retain their own structures and no structural distortion or steric hindrance was observed. Furthermore, the relative position of the LBT, as well as the La^{3+}, was reasonably defined against GB1. Thus, the present tagging method can be applied to a wide variety of proteins by introducing anchoring points based on the structures of the LBT and target proteins.

Steady-state $\{^1H\}$-^{15}N NOE was measured to estimate the mobility of the LBT and GB1 moieties of L2GB (Fig. 2b). The NOE values for both moieties were more than 0.7, suggesting that both moieties are relatively fixed. Thus, it can be concluded that the two-point anchoring method is useful for fixing the LBT to target proteins.

^1H-^{15}N HSQC spectra of L2GB and L1GB complexed with lanthanide ions

^1H-^{15}N HSQC spectra of the ^{15}N-labeled L2GB and L1GB were recorded at 283 K in the presence of 1 equivalent of lanthanide ions (La^{3+}, Tb^{3+}, Er^{3+}, and Tm^{3+}), where La^{3+} was used as a diamagnetic reference. The addition of the paramagnetic lanthanide ions to the ^{15}N-labeled L2GB and L1GB induced PCSs (Fig. 3, and Supporting information Table S1). Er^{3+} and Tm^{3+} induced signal shifts toward the

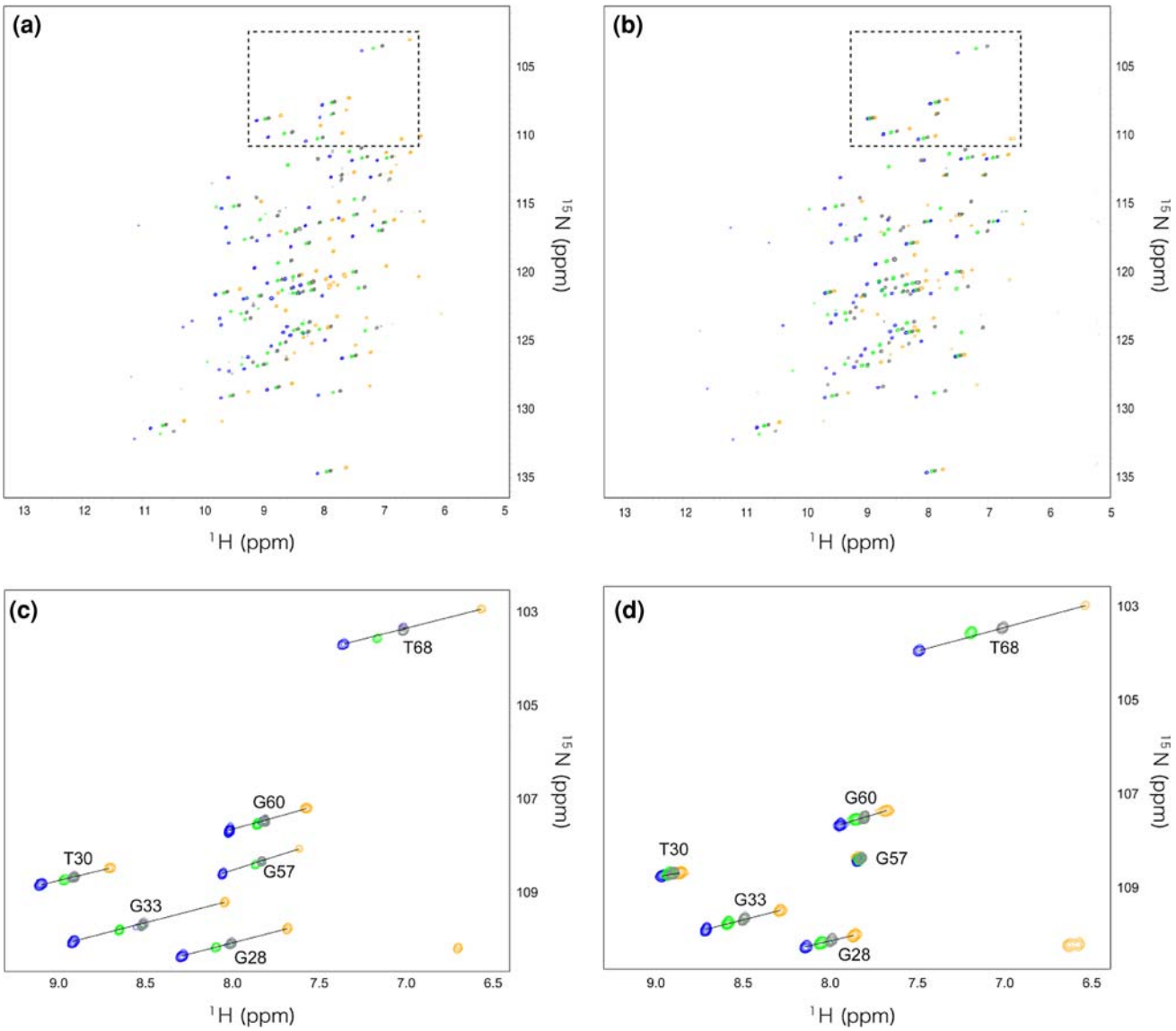

Fig. 3 ^1H-^{15}N HSQC spectra of ^{15}N L2GB (**a**) and ^{15}N L1GB (**b**) in complex with La^{3+} (*gray*), Er^{3+} (*green*), Tm^{3+} (*blue*), Tb^{3+} (*orange*). Expanded view of the region surrounded by *dashed line* in the spectra of L2GB (**c**) and L1GB (**d**). Spectra were acquired by 600 MHz NMR spectrometer at 283 K

lower field, and Tb^{3+} induced signal shifts toward the higher field. Although the signals from the amide protons close to the anchoring points of the LBT disappeared due to the paramagnetic relaxation effect, other signals were relatively sharp even in the presence of the strong paramagnetic lanthanide, Tb^{3+}.

$\Delta\chi$-tensors of paramagnetic lanthanide ions in L2GB and L1GB

Prior to the tensor calculations, the ^{1}H-^{15}N HSQC cross-peaks of the paramagnetic samples were assigned based on the diamagnetic spectrum. Since the ^{1}H and ^{15}N atoms of each amide group are close in space, the PCS had similar ppm values in both ^{1}H and ^{15}N dimensions (Su et al. 2006). Thus, most signals in the ^{1}H-^{15}N HSQC spectra of the paramagnetic samples were assigned based on those of the diamagnetic sample. Signals that remained unassigned after the manual assignment were additionally assigned using the Echidna program (Schmitz et al. 2006), for which the structure of L2GB, the peak table of the paramagnetic ^{1}H-^{15}N HSQC with incomplete assignments and assignments of the diamagnetic ^{1}H-^{15}N HSQC spectrum were used as input data.

The $\Delta\chi$-tensors were then calculated based on the PCS values and the structure of L2GB using the Numbat program (Schmitz et al. 2008; Table 2). For calculating the tensors, the metal position was also optimized based on the PCS values. The optimized metal position of L2GB was located 5.4 Å away from the position determined by CYANA. The $\Delta\chi_{ax}$ values in L1GB and L2GB were similar, while the $\Delta\chi_{rh}$ values in L1GB was appreciably smaller than those in L2GB. The correlations between experimental and back-calculated PCS values for L2GB and L1GB were both good, whereas the principal axis of the tensor were better defined in L2GB than in L1GB, as shown in the Sanson–Flamsteed plot (Fig. 4, and

Table 2 Magnetic susceptibility tensors of lanthanide ions in complex with L2GB and L1GB

	Lanthanide	$\Delta\chi^{a}_{ax}$	$\Delta\chi^{a}_{rh}$	α^{b}	β^{b}	γ^{b}
L2GB	Er^{3+}	−8.3 ± 0.7	−6.6 ± 0.2	190	142	152
	Tm^{3+}	−21.2 ± 2.7	−15.0 ± 1.1	167	131	120
	Tb^{3+}	32.4 ± 2.9	15.0 ± 1.6	174	134	133
L1GB	Er^{3+}	−7.5 ± 0.3	−3.9 ± 0.3	259	168	306
	Tm^{3+}	−19.2 ± 1.6	−10.2 ± 1.1	232	163	284
	Tb^{3+}	25.3 ± 1.4	5.1 ± 1.3	214	143	264

[a] $\Delta\chi_{ax}$ and $\Delta\chi_{rh}$ values are in 10^{-32} [m^3] and error estimates were obtained by Monte-Carlo protocol using the 100 partial PCS data sets in which 30% of the input data were randomly deleted

[b] The Euler angles (α, β, γ) are represented in ZXZ convention in degrees

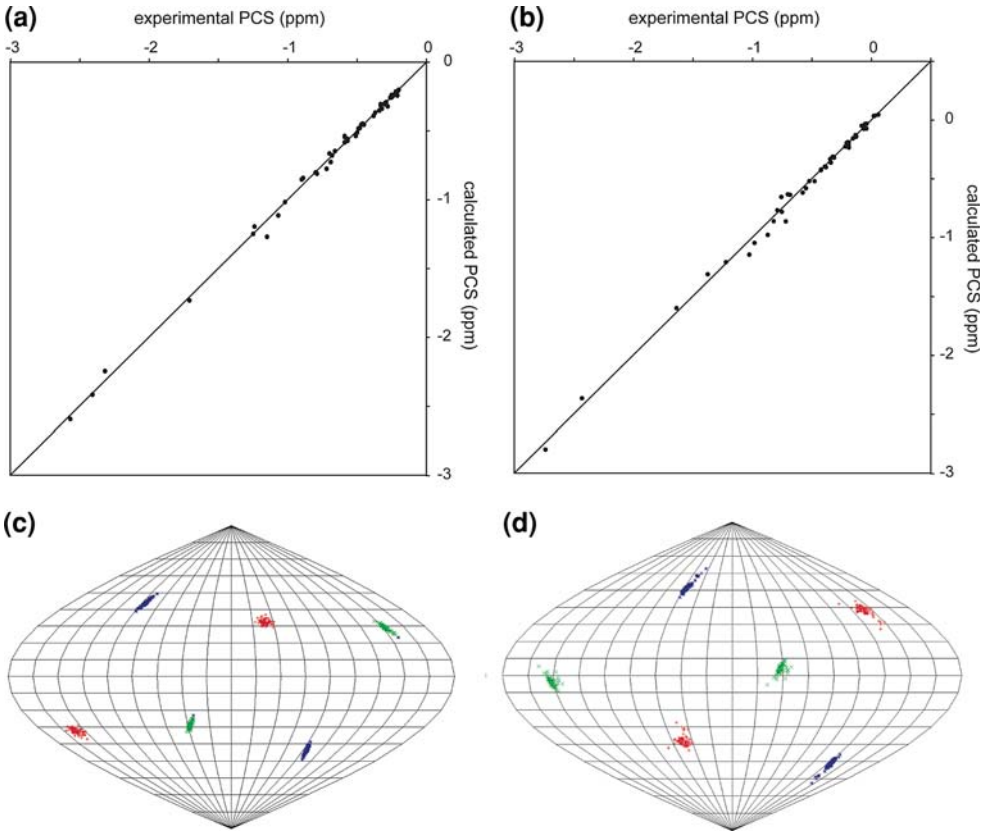

Fig. 4 Comparison between experimental and back-calculated PCS of backbone amide protons observed in L2GB (**a**) and L1GB (**b**) in the presence of Tb^{3+}. The ideal correlations are indicated. Orientation of the principal axis of the magnetic susceptibility tensor of Tb^{3+} in complex with L2GB (**c**) and L1GB (**d**), visualized in Sanson–Flamsteed projection. The plots show the points where the principal axis of the $\Delta\chi$-tensor penetrate the *sphere*, with the *z*-, *y*- and *x*-axis in *blue*, *green* and *red*, respectively. 100 sets of plots represent the result of Monte-Carlo analysis using the 100 partial PCS data sets in which 30% of the input data were randomly deleted

Supporting information Figures S2, S3). From these data, we concluded that the lanthanide ion is more fixed in L2GB than in L1GB and the reduced $\Delta\chi_{rh}$ tensor value in L1GB is possibly due to mobility around the axis of symmetry of the $\Delta\chi$-tensor in L1GB.

Unexpectedly, the PCS values of L2GB and L1GB did not differ greatly and, in fact, some L1GB signals showed larger PCS values than did those in L2GB (Table S1). However, the $\Delta\chi_{rh}$ values indicated that the lanthanide ion was fixed more rigidly in L2GB than in L1GB. This can be explained by differences in the metal position and the orientation of the principal axis of the $\Delta\chi$-tensor between L2GB and L1GB. The metal position in L1GB was closer to the GB1 moiety than that in L2GB; i.e., the distance between the metal and the sulfur atom of the cysteine residue was 10.1 Å in L1GB and 12.7 Å in L2GB. N-terminal fusion of the LBT slightly increased the distance of the metal from the GB1 moiety, which decreased the observed PCS value in L2GB.

RDC measurement and calculation of alignment tensors

We measured the RDC values for L2GB and L1GB in complex with Tm^{3+}, Er^{3+}, and Tb^{3+}, using a Varian UNITY Inova 600 MHz NMR spectrometer (Fig. 5a, b, and Supporting information Figure S4). As was consistent with the PCS measurement, the RDC induced by Tb^{3+} was of an opposite sign to those induced by Er^{3+} and Tm^{3+}, reflecting the different orientation of the anisotropy tensors. It is worth noting that the RDC values observed for L2GB were about 2–3 times larger than those for L1GB (Fig. 5).

Alignment tensors for L2GB and L1GB with Tm^{3+}, Er^{3+} and Tb^{3+} were calculated based on the RDC values and the structure of GB1 (PDB code 1gb1; Gronenborn et al. 1991), using Eq. 2 in the Module program (Dosset et al. 2001; Table 3; Fig. 5c, d). As predicted from the RDC values, the A_{ax} and A_{rh} components for L2GB were 2–3 times larger than those for L1GB. The mobility of the lanthanide-binding tag, and thus the mobility of the lanthanide ion, averaged the anisotropic effect of the lanthanide ion, which decreased the RDC values and the size of the alignment tensors (Bertini et al. 2004, 2007). Thus, taking the PCS and RDC analyses together, we concluded that the two-point anchoring of the LBT to GB1 reduced the mobility of the lanthanide ion more efficiently than did the single-point anchoring.

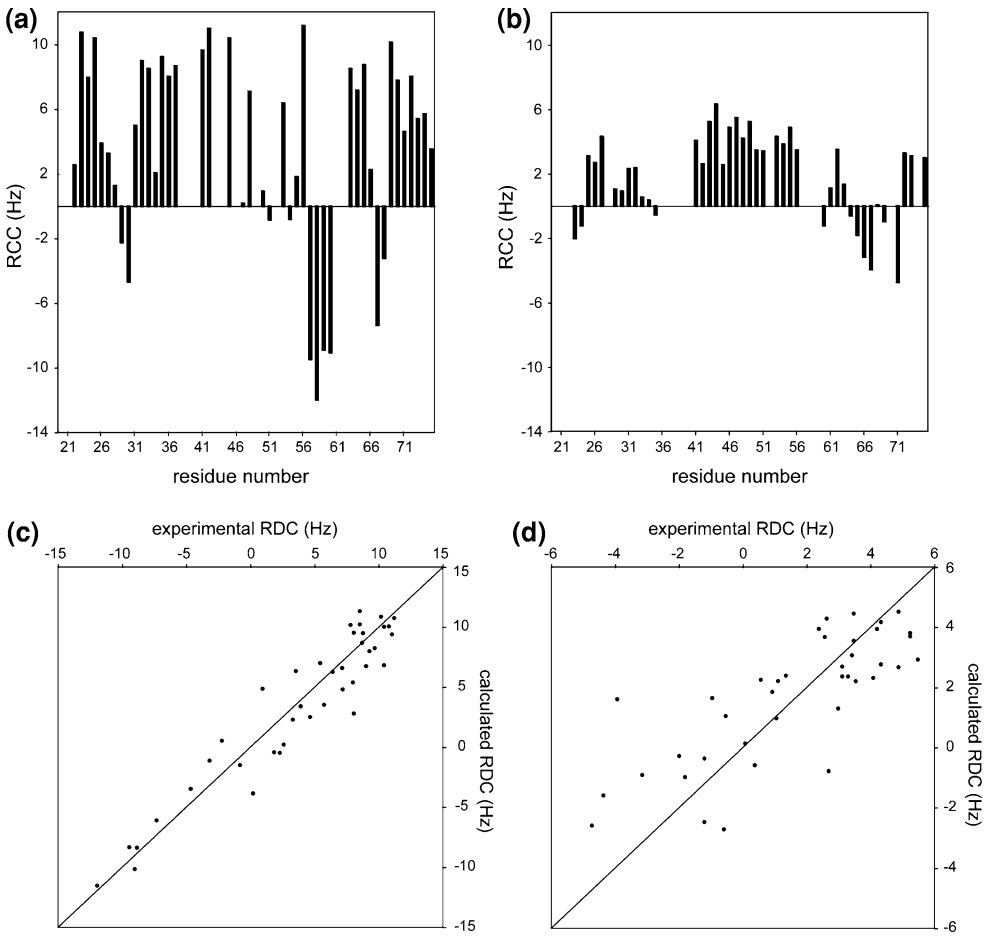

Fig. 5 RDC of L2GB (**a**) and L1GB (**b**) with Tb^{3+} plotted against the residue number. Spectra were acquired using 600 MHz NMR spectrometer at 283 K. The residue numbering for L1GB is represented to correspond to L2GB. Comparison between experimental and back-calculated RDC of backbone amide protons observed in L2GB (**c**) and L1GB (**d**) in the presence of Tb^{3+}. The ideal correlations are indicated

Comparison of anisotropic tensors derived from PCS and RDC data

The difference in the anisotropic effects between L2GB and L1GB was larger for the RDC-derived parameters than for the PCS-derived parameters; i.e., the PCS values and the $\Delta\chi$-tensors determined from the PCS data did not differ greatly between L2GB and L1GB, whereas there were two to threefold differences in the RDC values and the alignment tensors determined from the RDC data between L2GB and L1GB (Tables 2, 3; Fig. 5, and Supporting information Figure S4). It appears that RDC is more sensitive to the mobility of the lanthanide ion than is PCS (Keizers et al. 2007, 2008). For a comparison between the PCS and RDC datasets, the alignment tensors of L1GB and L2GB were converted to the $\Delta\chi$-tensors by Eq. 3,

$$\Delta\chi_{\mathrm{ax,rh}} = \frac{15\mu_0 k_{\mathrm{B}} T}{B_0^2} A_{\mathrm{ax,rh}}, \tag{3}$$

where B_0 is the magnetic field strength, k_{B} is the Boltzmann constant and T is the observed temperature (Supporting information Table S2). Results showed that $\Delta\chi_{\mathrm{ax}}^{\mathrm{RDC}}$ was 50–60% of $\Delta\chi_{\mathrm{ax}}^{\mathrm{PCS}}$ for L2GB, and about 25% for L1GB. The $\Delta\chi$-tensors obtained by RDC are generally smaller than those obtained by PCS, and they become even smaller when the structure is used for the tensor fitting without RDC-based refinement (Su et al. 2008a, b; Keizers et al. 2008). We did not refine the structure using RDC values, but used the GB1 structure determined by NOE constraints. If the RDC-refined structure is used in the tensor calculation, tensor values might be increased by more than 30% (Keizers et al. 2008). However, this is not sufficient to explain the present discrepancy. It is probable that the tag still has some mobility even in L2GB. In the L2GB structure, the orientation of the LBT with respect to GB1 is not absolutely defined, which might represent an actual fluctuation of the LBT as is shown in Fig. 2a. The simulation by Bertini et al. indicated that the averaging caused by the mobility of the principal axis of the tensor was more severe for RDC than for PCS (Bertini et al. 2004) and the experimental data also support this result (Bertini et al. 2007). There are several reports of similar discrepancies between PCS- and RDC-derived tensors associated with lanthanide tagging methods (Gaponenko et al. 2002), and even in metalloproteins (Banci et al. 1998; Déméné et al. 2000). In these cases, however, the structures were determined based on PCS and/or RDC data (Hus et al. 2000; Gaponenko et al. 2004).

Table 3 Alignment tensors of lanthanide ions in complex with the L2GB and L1GB as determined from RDC

	Lanthanide	$A_{\mathrm{ax}}^{\mathrm{a}}$	$A_{\mathrm{rh}}^{\mathrm{a}}$	α^{b}	β^{b}	γ^{b}
L2GB	Er^{3+}	−1.08 ± 0.18	−0.84 ± 0.35	175	126	234
	Tm^{3+}	−2.93 ± 0.16	−2.41 ± 0.36	179	123	251
	Tb^{3+}	4.92 ± 0.21	3.20 ± 0.37	112	119	160
L1GB	Er^{3+}	−0.54 ± 0.17	−0.61 ± 0.31	185	106	233
	Tm^{3+}	−1.33 ± 0.18	−1.38 ± 0.44	180	94	228
	Tb^{3+}	1.77 ± 0.19	1.15 ± 0.40	135	99	183

[a] A_{ax} and A_{rh} values are in 10^{-4} and error estimates were obtained by Monte-Carlo based analysis using 100 replicate RDC data sets with Gaussian noise

[b] The Euler angles (α, β, γ) are represented in ZXZ convention in degrees

Application of PCS for structure calculation

To validate the applicability of the two-point attachment of the LBT for structural analysis, we calculated the structure of the GB1 moiety of L2GB using the PCS restraints as well as the NOE derived distance restraints. Since convergence of the structure of GB1 was satisfactory even in the absence of the paramagnetic restraints (Fig. 2a), we used a limited number of the NOE constraints in which 50% of the NOE restraints were randomly deleted. Using Paramagnetic CYANA (Banci et al. 1998), the structures of GB1 were calculated based on a total of 602 inter-proton distance restraints with or without 160 PCS restraints observed for backbone amide protons of GB1 obtained in the presence of Er^{3+}, Tm^{3+} and Tb^{3+}. The structure was improved by using the PCS restraints, where the structures with PCS restraints had an average backbone RMSD of 0.93 Å and those without PCS restraints had RMSD of 1.23 Å (Supporting information Figure S5). This result indicates that the present tagging method can be applied to structural analysis.

Comparison of synthetic lanthanide chelators with two-point anchoring

Rigidity of the tag is important for the acquisition of accurate structural information with a minimum of experimental error and artifact. Two-point anchoring of the tag is efficient in reducing tag mobility. The symmetrically designed synthetic chelators can be anchored to the protein via two disulfide bonds (Rodriguez-Castañeda et al. 2006; Vlasie et al. 2007; Keizers et al. 2007, 2008; Prudêncio et al. 2004). However, most of these synthetic tags show peak doubling due to enantiomeric conformer of the lanthanide-substituted tag. The lanthanide binding peptide tags (LBTs) have advantages over the synthetic tags, in terms of availability, chiral purity and rigidity because of their bulkiness (Su et al. 2008a). Here, we introduced the lanthanide binding peptide tag with two-point anchoring which improved the rigidity of the tag against the protein and provided larger RDC values and the $\Delta\chi$-tensor.

Furthermore, it was shown that the structure of the GB1 was successfully refined using the PCS restraints derived from the two-point anchored LBT. Further studies may be needed to investigate the combined use of the PCS and RDC, as the residual mobility of the tag appears to have a relatively larger influence on RDC. However, the two-point anchoring tag is useful at least for the separate exploitation of RDC and PCS, as the magnitude of the RDC was much larger and the $\Delta\chi$-tensor derived from PCS was comparable to that of calbindin (Bertini et al. 2001a) with similar coordination sites around the lanthanide ions.

It should be mentioned that Keizers et al. recently reported the double-anchored chelator which provided good agreement between $\Delta\chi^{PCS}$ and $\Delta\chi^{RDC}$: $\Delta\chi^{RDC}_{ax}$ was 60–90% of $\Delta\chi^{PCS}_{ax}$, indicating higher rigidity of this tag (Keizers et al. 2007, 2008).

Conclusion

We have shown that the lanthanide-binding peptide tag linked to the target protein via two anchoring points, a disulfide bridge and an N-terminal fusion, reduces the mobility of the tag and is useful for the wide application of the lanthanide ions to the structural analysis of non-metalloproteins. This tagging method has several advantages in terms of (1) availability for protein NMR researchers, (2) chiral purity, (3) maintenance of the target protein structure, and (4) increased rigidity of tag compared to single-point anchoring. This two-point anchoring method was applied to GB1, thereafter referred to as L2GB. L2GB provided PCS values of up to 2.7 ppm in complex with Tm^{3+}, and RDC values in the range of -12 to $+11$ Hz when measured by 600 MHz NMR spectrometer in complex with Tb^{3+}. The rhombicity of the magnetic susceptibility tensor determined on the basis of the PCS values was much larger than that of L1GB. Furthermore, L2GB provided RDC values and alignment tensors almost twice as large as those of L1GB. These data indicate that the two-point tagging of the LBT efficiently reduced the mobility of the lanthanide ion. It was also shown that PCS restraints obtained from L2GB were successfully used in the early stage of structure determination: the average backbone RMSD was reduced from 1.23 Å to 0.93 Å for GB1.

References

Allegrozzi M, Bertini I, Janik MBL, Lee YM, Liu G, Luchinat C (2000) Lanthanide-induced pseudocontact shifts for solution structure refinements of macromolecules in shells up to 40 Å from the metal ion. J Am Chem Soc 122:4154–4161

Banci L, Bertini I, Huber JG, Luchinat C, Rosato A (1998) Partial orientation of oxidized and reduced cytochrome b5 at high magnetic fields: magnetic susceptibility anisotropy contributions and consequences for protein solution structure determination. J Am Chem Soc 120:12903–12909

Barbieri R, Bertini I, Cavallaro G, Lee YM, Luchinat C, Rosato A (2002) Paramagnetically induced residual dipolar couplings for solution structure determination of lanthanide binding proteins. J Am Chem Soc 124:5581–5587

Battiste JL, Wagner G (2000) Utilization of site-directed spin labeling and high-resolution heteronuclear nuclear magnetic resonance for global fold determination of large proteins with limited nuclear overhauser effect data. Biochemistry 39:5355–5365

Bertini I, Janik MB, Lee YM, Luchinat C, Rosato A (2001a) Magnetic susceptibility tensor anisotropies for a lanthanide ion series in a fixed protein matrix. J Am Chem Soc 123:4181–4188

Bertini I, Janik MB, Liu G, Luchinat C, Rosato A (2001b) Solution structure calculations through self-orientation in a magnetic field of a cerium(III) substituted calcium-binding protein. J Magn Reson 148:23–30

Bertini I, Del Bianco C, Gelis I, Katsaros N, Luchinat C, Parigi G, Peana M, Provenzani A, Zoroddu MA (2004) Experimentally exploring the conformational space sampled by domain reorientation in calmodulin. Proc Natl Acad Sci USA 101:6841–6846

Bertini I, Luchinat C, Parigi G, Pierattelli R (2005) NMR spectroscopy of paramagnetic metalloproteins. Chembiochem 6:1536–1549

Bertini I, Gupta YK, Luchinat C, Parigi G, Peana M, Sgheri L, Yuan J (2007) Paramagnetism-based NMR restraints provide maximum allowed probabilities for the different conformations of partially independent protein domains. J Am Chem Soc 129:12786–12794

Bertini I, Luchinat C, Parigi G, Pierattelli R (2008) Perspectives in paramagnetic NMR of metalloproteins. Dalton Trans 29:3782–3790

Cornilescu G, Delaglio F, Bax A (1999) Protein backbone angle restraints from searching a database for chemical shift and sequence homology. J Biomol NMR 13:289–302

DeLano WL (2002) The PyMOL molecular graphics system. Palo Alto, CA

Déméné H, Tsan P, Gans P, Marion D (2000) NMR determination of the magnetic susceptibility anisotropy of cytochrome c' of rhodobacter capsulatus by 1JHN dipolar coupling constants measurement: characterization of its monomeric state in solution. J Phys Chem B 104:2559–2569

Dosset P, Hus JC, Marion D, Blackledge M (2001) A novel interactive tool for rigid-body modeling of multi-domain macromolecules using residual dipolar couplings. J Biomol NMR 20:223–231

Dvoretsky A, Gaponenko V, Rosevear PR (2002) Derivation of structural restraints using a thiol-reactive chelator. FEBS Lett 528:189–192

Gaponenko V, Dvoretsky A, Walsby C, Hoffman BM, Rosevear PR (2000) Calculation of z-coordinates and orientational restraints using a metal binding tag. Biochemistry 39:15217–15224

Gaponenko V, Altieri AS, Li J, Byrd RA (2002) Breaking symmetry in the structure determination of (large) symmetric protein dimers. J Biomol NMR 24:143–148

Gaponenko V, Sarma SP, Altieri AS, Horita DA, Li J, Byrd RA (2004) Improving the accuracy of NMR structures of large proteins using pseudocontact shifts as long-range restraints. J Biomol NMR 28:205–212

Gronenborn AM, Filpula DR, Essig NZ, Achari A, Whitlow M, Wingfield PT, Clore GM (1991) A novel, highly stable fold of the immunoglobulin binding domain of streptococcal protein G. Science 254:581–582

Haberz P, Rodriguez-Castañeda F, Junker J, Becker S, Leonov A, Griesinger C (2006) Two new chiral EDTA-based metal chelates for weak alignment of proteins in solution. Org Lett 8:1275–1278

Herrmann T, Güntert P, Wüthrich K (2002) Protein NMR structure determination with automated NOE assignment using the new software CANDID and the torsion angle dynamics algorithm DYANA. J Mol Biol 319:209–227

Hus JC, Marion D, Blackledge M (2000) De novo determination of protein structure by NMR using orientational and long-range order restraints. J Mol Biol 298:927–936

Ikegami T, Verdier L, Sakhaii P, Grimme S, Pescatore B, Saxena K, Fiebig KM, Griesinger C (2004) Novel techniques for weak alignment of proteins in solution using chemical tags coordinating lanthanide ions. J Biomol NMR 29:339–349

Keizers PH, Desreux JF, Overhand M, Ubbink M (2007) Increased paramagnetic effect of a lanthanide protein probe by two-point attachment. J Am Chem Soc 129:9292–9293

Keizers PH, Saragliadis A, Hiruma Y, Overhand M, Ubbink M (2008) Design, synthesis, and evaluation of a lanthanide chelating protein probe: CLaNP-5 yields predictable paramagnetic effects independent of environment. J Am Chem Soc 130:14802–14812

Koradi R, Billeter M, Wüthrich K (1996) MOLMOL: a program for display and analysis of macromolecular structures. J Mol Graph 14:51–55

Leonov A, Voigt B, Rodriguez-Castañeda F, Sakhaii P, Griesinger C (2005) Convenient synthesis of multifunctional EDTA-based chiral metal chelates substituted with an S-mesylcysteine. Chem Eur J 11:3342–3348

Ma C, Opella SJ (2000) Lanthanide ions bind specifically to an added "EF-hand" and orient a membrane protein in micelles for solution NMR spectroscopy. J Magn Reson 146:381–384

Martin LJ, Hähnke MJ, Nitz M, Wöhnert J, Silvaggi NR, Allen KN, Schwalbe H, Imperiali B (2007) Double-lanthanide-binding tags: design, photophysical properties, and NMR applications. J Am Chem Soc 129:7106–7113

Nitz M, Franz KJ, Maglathlin RL, Imperiali B (2003) A powerful combinatorial screen to identify high-affinity terbium(III)-binding peptides. Chembiochem 4:272–276

Nitz M, Sherawat M, Franz KJ, Peisach E, Allen KN, Imperiali B (2004) Structural origin of the high affinity of a chemically evolved lanthanide-binding peptide. Angew Chem Int Ed Engl 12:3682–3685

Otting G (2008) Prospects for lanthanides in structural biology by NMR. J Biomol NMR 2008(4):1–9

Pintacuda G, Moshref A, Leonchiks A, Sharipo A, Otting G (2004) Site-specific labelling with a metal chelator for protein-structure refinement. J Biomol NMR 29:351–361

Pintacuda G, Park AY, Keniry MA, Dixon NE, Otting G (2006) Lanthanide labeling offers fast NMR approach to 3D structure determinations of protein-protein complexes. J Am Chem Soc 2006(128):3696–3702

Pintacuda G, John M, Su XC, Otting G (2007) NMR structure of protein-ligand complexes by lanthanide labeling. Acc Chem Res 40:206–212

Prudêncio M, Rohovec J, Peters JA, Tocheva E, Boulanger MJ, Murphy ME, Hupkes HJ, Kosters W, Impagliazzo A, Ubbink M (2004) A caged lanthanide complex as a paramagnetic shift agent for protein NMR. Chemistry 10:3252–3260

Rodriguez-Castañeda F, Haberz P, Leonov A, Griesinger C (2006) Paramagnetic tagging of diamagnetic proteins for solution NMR. Magn Reson Chem 44:S10–S16

Rumpel S, Becker S, Zweckstetter M (2007) High-resolution structure determination of the CylR2 homodimer using paramagnetic relaxation enhancement and structure-based prediction of molecular alignment. J Biomol NMR 40:1–13

Saio T, Kumeta H, Ogura K, Yokochi M, Asayama M, Katoh S, Katoh E, Teshima K, Inagaki F (2007) The cooperative role of OsCnfU-1A domain I and domain II in the iron sulphur cluster transfer process as revealed by NMR. J Biochem 142:113–121

Schmitz C, John M, Park AY, Dixon NE, Otting G, Pintacuda G, Huber T (2006) Efficient chi-tensor determination and NH assignment of paramagnetic proteins. J Biomol NMR 35:79–87

Schmitz C, Stanton-Cook MJ, Su XC, Otting G, Huber T (2008) Numbat: an interactive software tool for fitting deltachi-tensors to molecular coordinates using pseudocontact shifts. J Biomol NMR 41:179–189

Su XC, Huber T, Dixon NE, Otting G (2006) Site-Specific Labelling of Proteins with a Rigid Lanthanide-Binding Tag. ChemBioChem 7:1599–1604

Su XC, McAndrew K, Huber T, Otting G (2008a) Lanthanide-binding peptides for NMR measurements of residual dipolar couplings and paramagnetic effects from multiple angles. J Am Chem Soc 130:1681–1687

Su XC, Man B, Beeren S, Liang H, Simonsen S, Schmitz C, Huber T, Messerle BA, Otting G (2008b) A dipicolinic acid tag for rigid lanthanide tagging of proteins and paramagnetic NMR spectroscopy. J Am Chem Soc 130:10486–10487

Tang C, Schwieters CD, Clore GM (2006) Open-to-closed transition in apo maltose-binding protein observed by paramagnetic NMR. Nature 449:1078–1082

Vlasie MD, Comuzzi C, van den Nieuwendijk AM, Prudêncio M, Overhand M, Ubbink M (2007) Long-range-distance NMR effects in a protein labeled with a lanthanide-DOTA chelate. Chem Eur J 13:1715–1723

Vlasie MD, Fernández-Busnadiego R, Prudêncio M, Ubbink M (2008) Conformation of pseudoazurin in the 152 kDa electron transfer complex with nitrite reductase determined by paramagnetic NMR. J Mol Biol 375:1405–1415

Wöhnert J, Franz KJ, Nitz M, Imperiali B, Schwalbe H (2003) Protein alignment by a coexpressed lanthanide-binding tag for the measurement of residual dipolar couplings. J Am Chem Soc 125:13338–13339

Zhuang T, Lee HS, Imperiali B, Prestegard JH (2008) Structure determination of a galectin-3-carbohydrate complex using paramagnetism-based NMR constraints. Protein Sci 17:1220–1231